nature chemistry

ARTICLES

PUBLISHED ONLINE: 23 MAY 2011 | DOI: 10.1038/NCHEM.1046

A microdroplet dilutor for high-throughput screening

Xize Niu, Fabrice Gielen, Joshua B. Edel* and Andrew J. deMello*†

Pipetting and dilution are universal processes used in chemical and biological laboratories to assay and experiment. In microfluidics such operations are equally in demand, but difficult to implement. Recently, droplet-based microfluidics has emerged as an exciting new platform for high-throughput experimentation. However, it is challenging to vary the concentration of droplets rapidly and controllably. To this end, we developed a dilution module for high-throughput screening using droplet-based microfluidics. Briefly, a nanolitre-sized sample droplet of defined concentration is trapped within a microfluidic chamber. Through a process of droplet merging, mixing and re-splitting, this droplet is combined with a series of smaller buffer droplets to generate a sequence of output droplets that define a digital concentration gradient. Importantly, the formed droplets can be merged with other reagent droplets to enable rapid chemical and biological screens. As a proof of concept, we used the dilutor to perform a high-throughput homogeneous DNA-binding assay using only nanolitres of sample.

High-throughput screening can provide an enormous amount of information on the utility of the components of molecular libraries and is now guiding research directions in diverse areas, ranging from directed evolution to small-molecule synthesis[1,2]. The key parameters that determine the efficiency of such exploration processes are the sample volumes required per screen and the number of reagent combinations that can be examined per unit time. Currently, exploration of molecular diversity is only possible with substantial investment in liquid-handling robots (and their associated infrastructure) that perform screens in microwell plates. Microwell plates are typically open plastic substrates with between 96 and 3,456 sample wells arranged in a 2:3 rectangular matrix. Based on a standard footprint, each well can hold a volume that ranges from tens of nanolitres to several millilitres of liquid. This general automated approach affords screening capacities of $<10^4$ samples per day, utilizes sample and reagent volumes in the order of tens of microlitres and requires a capital investment of tens of millions US dollars.

An attractive alternative to conventional laboratory-based screening technologies involves the adoption of microfluidic or lab-on-a-chip technologies. Recent years have seen considerable progress in the development of such microfabricated systems for use in the chemical and biological sciences[3,4]. Much of this development was driven by a need to perform rapid analytical or synthetic operations on small volumes of sample[5]. However, at a more basic level, the appeal of miniaturized analytical systems is motivated by the fact that physical and chemical processes can be controlled and harnessed more easily when instrumental dimensions are reduced to the micron (or submicron) scale. In the current context, such systems define new operational paradigms and have the potential to transform high-throughput synthesis and compound-library screening. For example, Quake and co-workers pioneered the development of microfluidic large-scale integration and described the use of microfluidic devices that contain thousands of micromechanical valves and hundreds of individually addressable reaction chambers[6–8].

A fundamental and non-trivial challenge associated with the application of microfluidic technology to high-throughput screening is the ability to control and vary the concentration of the analytical sample under investigation. Although this is a standard and simple pipetting operation on the macroscale, the formation of discrete samples of varying concentrations within a microfluidic system is surprisingly challenging. Whitesides and co-workers addressed the problem of concentration-gradient generation in continuous-flow microfluidic systems by exploiting laminar flows[9]. Specifically, the authors utilized controlled diffusive mixing of species flowing in parallel fluid streams. This approach was refined to allow the production of complex spatial and temporal concentration gradients and has been applied to a diversity of chemical and biological systems[10,11].

Unfortunately, the use of such gradient generators is not ideal in situations where multiple, discrete assays need to be performed with high throughput and in a quantitative fashion, because the formed gradients exist in a continuous phase. Indeed, the screening of multiple reactions (or compounds) remains a critical challenge in single-phase microfluidic systems, where sample volumes are restricted (nanolitres to microlitres), and analyte diffusion and Taylor dispersion tend to expand the formed concentration distributions[12]. Moreover, the problems associated with the non-specific binding of reagents to channel surfaces pose serious issues for cross-contamination in any high-throughput approach[13].

In recent years, droplet-based (or segmented flow) microfluidics has emerged as a potential new platform for high-throughput and high-efficiency experimentation in biology and chemistry[14,15]. In simple terms, droplets or plugs can be made to develop spontaneously when multiple lamina streams of aqueous reagents are injected into an immiscible carrier fluid. Importantly, droplets formed in this way have nano- to picolitre volumes, are isolated from channel surfaces and other droplets, and can be manufactured at kilohertz frequencies[16]. Unlike continuous-flow microfluidic systems, processed reagents can be encapsulated or digitized within the carrier phase, allowing for independent control of each

Department of Chemistry, Imperial College London, Exhibition Road, South Kensington, London SW7 2AZ, UK.; †Present address: Department of Chemistry and Applied Biosciences, Institute for Chemical and Bioengineering, ETH Zürich, HCI E125, Wolfgang Pauli Strasse 10, CH-8093 Zürich, Switzerland.
*e-mail: Joshua.edel@imperial.ac.uk; andrew.demello@chem.ethz.ch

droplet. Accordingly, there exists an opportunity to generate, order, maintain and utilize sequences of droplets that contain a given analyte at varying concentrations. In the mass production of droplets using microfluidic T-junctions or flow-focusing geometries, the variation of volumetric flow-rate ratios (of the aqueous inputs) during the droplet-formation process provides a direct way of changing the relative concentration of encapsulated reagents[17]. Unfortunately, in practice this approach suffers because flow stabilization occurs over a timescale of many seconds to minutes when using precision syringe pumps and, moreover, flow-rate variations can access only concentration ranges of approximately two orders of magnitude[17] (by Supplementary Fig. S1). Consequently, current approaches to high-throughput screening of reaction conditions using droplet-based microfluidics rely on extracting data from hundreds or thousands of droplets[18].

A distinct property for droplets travelling along microfluidic conduits is that they experience various hydrodynamic interactions[14], because capillary effects dominate viscous forces (capillary numbers range between 10^{-1} and 10^{-5} in most microfluidic systems). Accordingly, such spatial and temporal uncertainties require feedback schemes to realize reliable integrated valving or the implementation of other optical and electrical control tools[19], which significantly increases the level of system complexity. To overcome such difficulties, recent studies utilized the simultaneous transportation of materials with the use of logical control operations by leveraging the capillary effect. For example, bubble logic schemes[20], pillar structures for droplet merging[21,22], droplet selection according to size[23] and the manipulation of ultra-small sample volumes for analytical separations[24] are reported. To address the problems of controlling concentration in droplet-based microfluidics, we proposed an alternative strategy that is able to access concentration ranges in excess of four orders of magnitude, by utilizing water–oil hydrodynamic interactions and manipulating single-droplet interactions.

Results and discussion

Herein, we propose a passive platform that can achieve the controllable dilution of nanolitre samples dispersed within an immiscible phase. The approach is based on liquid–liquid and liquid–channel structure hydrodynamic interactions; a typical device structure is shown in Fig. 1a. The sequence of droplets used in the dilution studies presented can be generated using standard flow-focusing or T-junction approaches[16,25]. However, to screen multiple samples and explore the functionality and potential of the dilution chamber, it is favourable to pregenerate the droplet sequence from different reservoirs into the tubing with the desired volumes, sequences and intervals (in our experiments droplet volumes ranged from 500 pl to 5 nl). Then these droplets can be injected directly into the microdevice for screening. Once inside, the first 'high-concentration' sample droplet can be diluted through interaction with a sequence of subsequent droplets of lower (or zero) analyte concentration. The output of this generic process is a sequence of droplets that have different concentrations of the desired analyte. More specifically, the concentration diminishes in a logarithmic fashion as a function of droplet number, but maintains both droplet size and droplet spacing. The results of this procedure are shown in Fig. 1c. Unlike concentration gradients generated under continuous-flow conditions, the output units of the process described here are dissociated and therefore reagents are kept within individual droplets and can undergo further processing and analysis.

The detailed process of droplet dilution can be partitioned into four steps: droplet trapping, droplet merging, droplet resplitting and droplet mixing (within the trapped 'mother' droplet). Each component of this process is visualized in Fig. 1b. This dilution process is highly analogous to routine pipetting operations

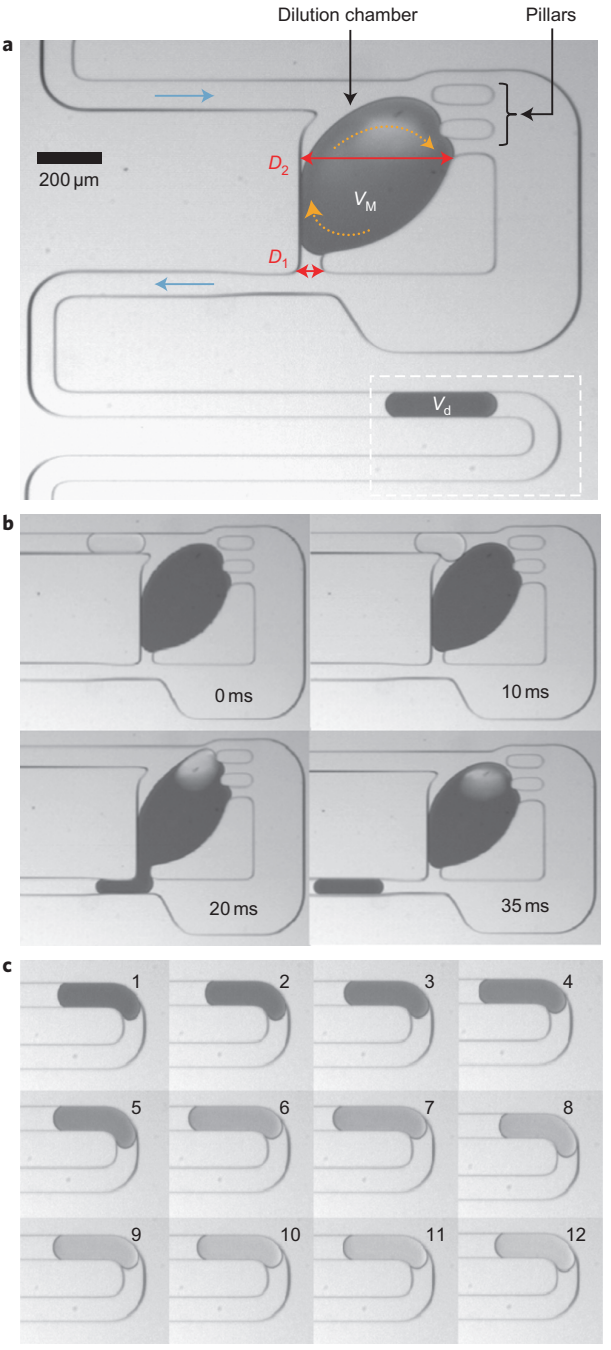

Figure 1 | Design and operation of the droplet dilutor. a, Schematic of the dilution module showing the input channel, the dilution chamber, pillar structures, the side channel and an extended output channel. The flow direction is indicated by blue arrows. A droplet that contains food dye is trapped inside the dilution chamber and forms the 'mother droplet'. The volume of the mother droplet is given by V_M and that of the output droplet by V_d. The dashed orange arrows indicate the recirculatory mixing within the mother droplet caused by the flow of the continuous phase. **b**, Process of sequential dilution. A buffer droplet approaches (0 ms), contacts the mother droplet (10 ms), coalesces and activates the soft valve (20 ms), and finally generates an output droplet (35 ms). Mixing within the mother droplet takes place during and after output-droplet generation. The high-speed Supplementary Movie S1 shows the entire process. **c**, Images of a sequence of droplets flowing through the output channel taken from the dashed rectangular box in (**a**). The concentration of dye in the output droplets decreases exponentially according to the droplet number n following $(1-V_d/V_M)^n$.

performed on the bench top, in which samples are aspirated into a certain volume, transported and dispensed into a container, where mixing with the container's contents affords dilution. Such a pipetting process can be repeated to perform a screen of various concentrations. In the experiments, our droplet dilutor operated with volumes between three and six orders of magnitude smaller than typically used in conventional pipetting and robotic screening. In the initial experiments the mother droplet and dilution droplets had volumes of 6 nl and 1 nl, respectively.

To locate and trap droplets, a dilution chamber was designed to have a smaller output channel width ($D_1 = 80$ μm) than the inlet part ($D_2 = 520$ μm), as shown in Fig. 1a. A liquid plug held inside the chamber was thus deformed and subjected to a back pressure (because of surface tension, Supplementary Fig. S3):

$$\Delta p_{\mathrm{surf}} \propto \gamma(2\cos(\theta+\alpha)/D_2 - 2\cos(\theta-\alpha)/D_1) \qquad (1)$$

Here γ is the interfacial tension (between 10 and 50 mN m^{-1} for a typical oil–aqueous system), θ is the contact angle of the droplet on the channel wall and α is the angle that defines the non-parallel channel walls between D_2 and D_1 (Supplementary Fig. S3). This yields a back pressure of between 10^1 and 10^2 Pa for the current liquid and channel dimensions. Such back pressures are normally insufficient to stop flows in simple channels that contain a pure expansion in width[26], because of the high hydraulic pressure required to drive the flow along the whole length of the microchannel[20]. However, by implementing a side channel in close proximity to the dilution chamber (Fig. 1a) that conducts the oil flow around the chamber, the hydraulic pressure that the droplet sustains can be decreased dramatically to:

$$\Delta p'_{\mathrm{hydraulic}} \propto \mu' L' Q/(h' w^3) \qquad (2)$$

Here μ' is the viscosity of the oil, L' the length of the droplet, Q the total flow rate and h' and w are the height and width of the side channel, respectively. Under typical conditions, the hydraulic pressure is between 1 and 100 Pa, which is equivalent to the back pressure induced by surface tension. Such local droplet manipulation is effective in droplet trapping, flip-flop memory or adjusting the distance between adjacent droplets in a flow[20,27]. Moreover, as both Δp_{surf} and $\Delta p'_{\mathrm{hydraulic}}$ are proportional to $1/L'$, such a local manipulation approach is valid for regimes of low capillary number and further reductions in feature size are feasible for droplet trapping.

With the depletion of oil through the side channels (that is, between the pillars), the subsequent droplet can merge readily with the mother droplet trapped inside the dilution chamber. Crucially, if the accumulated droplet (mother droplet + dilution droplet) becomes larger than the chamber volume, it will block the oil flow in the side channels and a portion of the combined droplet will be pushed out from the outlet, until the now-resumed oil flow cuts the extruded aqueous phase into a secondary droplet at the 'T' junction (Fig. 1b and Supplementary Movie S1). This means that the generation of an output droplet is triggered only by the merging of an input droplet with the mother droplet, which forms a 'soft valve' during the blockage and reopening of the oil flow. By sweeping the size of the input droplets from five times the volume of the mother droplet to one-tenth that of the mother droplet, we constructed a size comparison of the input droplets and the output drops. Supplementary Fig. S4 shows this relationship graphically, and demonstrates that the soft valve maintains the equality in input and output droplet volumes, and thus conserves the mother droplet volume. However, for the current design, when the input droplet volume is less than one-tenth that of the mother droplet volume, the soft valve does not function in a linear manner because the increased droplet volume cannot completely block the side-channel flow.

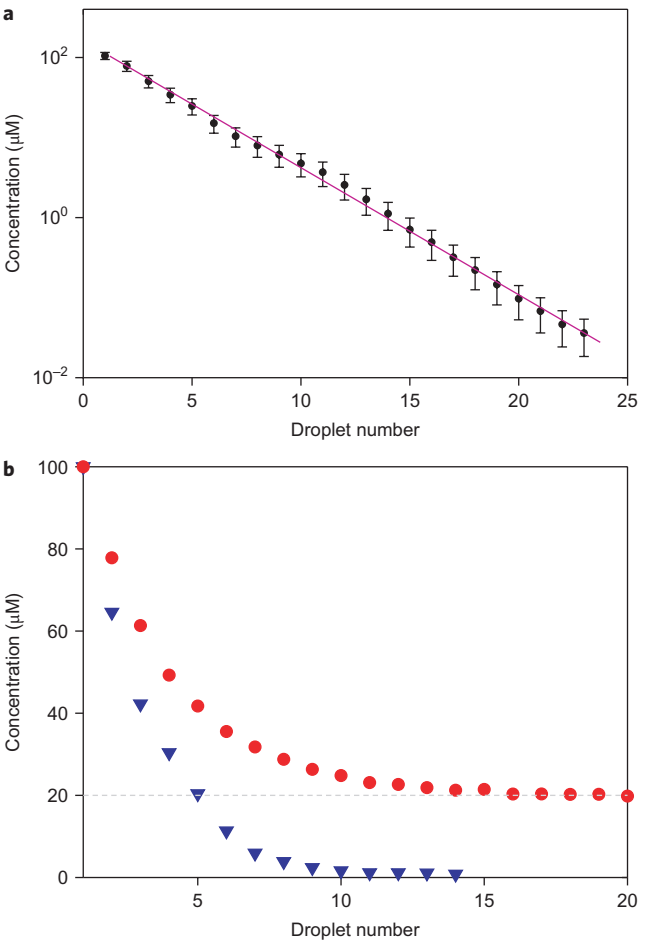

Figure 2 | Calibration of sequential dilution. a, Sequential dilution of a 6 nl mother droplet containing 100 μM fluorescein in water. The concentration of each output droplet was calculated from the recovered fluorescent signal. In this experiment, 23 output droplets accessed approximately four orders of magnitude in terms of concentration (100 μM to 36 nM). Error bars were calculated from the propagation of volume mismatches throughout the dilution process. **b**, Sequential dilution of a 100 μM fluorescein sample water droplet with different baselines. The triangles represent dilution with pure water input droplets and the circles represent dilution with aqueous input droplets composed of 20 μM fluorescein.

Careful inspection of Fig. 1b shows that during the resplitting process, fluid within the mother droplet moves in a laminar fashion with weak corner flows. This means that the newly merged droplet is kept wholly within the dilution chamber until the next droplet enters. Mixing of the newly merged droplet with the mother droplet occurs immediately after resplitting and relies on a 'moving wall' effect at the interface between the oil and the droplet. The viscous-drag force from the shearing of oil flow, $F \propto \mu h U$ (where μ is the viscosity of the aqueous phase, h is the height of the chamber and U is the average flow rate at the oil–water interface), induces circulation inside the mother droplet[28,29] and complete mixing is achieved within 500 ms at a total flow rate of 2 μl min^{-1}. Although this is slower than chaotic mixing in a droplet moving along a channel[30], a further increase in flow rate is expected to increase the mixing speed.

The dilution capability of the device was verified experimentally by forming a mother droplet with a 100 μM fluorescein solution and a sequence of smaller buffer droplets. A 488 nm excitation

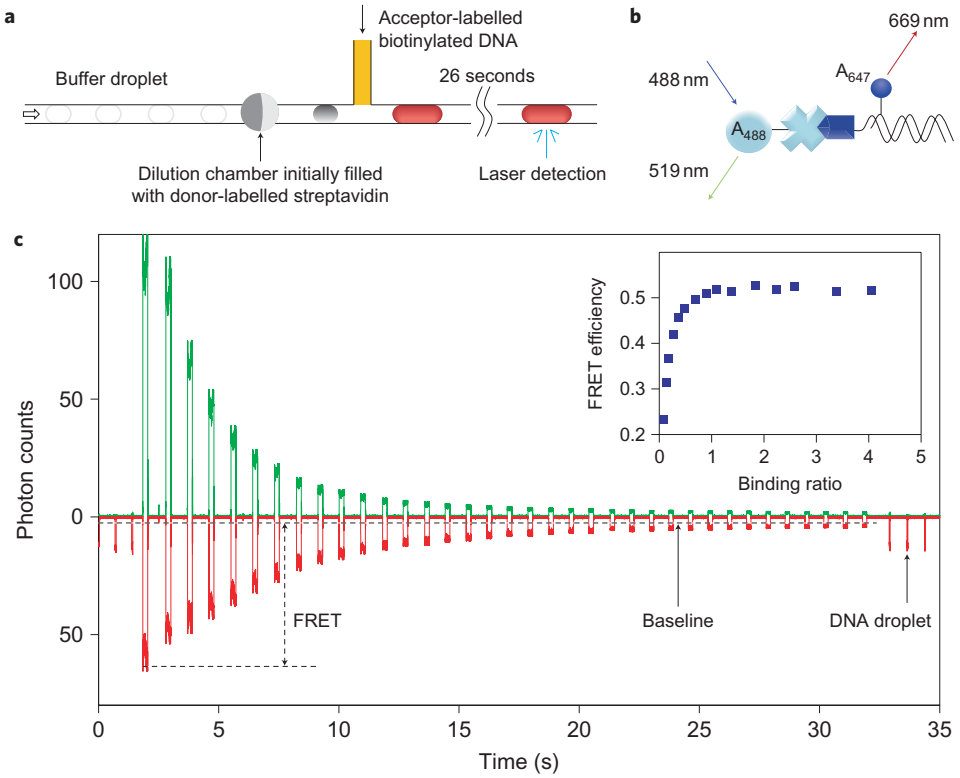

Figure 3 | Application of the droplet dilution module in a homogeneous DNA-binding assay. a, Schematic of the droplet dilution and further reaction. 100 nM streptavidin labelled with AF488 were diluted with buffer droplets that contained 100 mM Tris-HCl, 10 mM NaCl and 3 mM $MgCl_2$ at pH 8.0. The output droplets were merged with a continuous stream of AF647-labelled biotinylated oligonucleotide. The product droplet was flowed for 26 seconds through an incubation channel before optical detection. **b**, The FRET pair AF488–AF647 was brought into proximity through the biotin–streptavidin binding. **c**, Green and red fluorescent signals as detected by avalanche photodiode detectors for the donor and acceptor. Each peak represents one droplet. The baseline represents the red signal from AF647 in the absence of FRET. Its height is two-fifths of the signal of the DNA droplet alone, which correlates to the volumetric ratio between the DNA droplet and the merged droplet (DNA droplet plus buffer droplet). The red signal above the baseline corresponds to FRET events. The complete screening was performed within 30 seconds with 30 droplets. Inset: the binding curve illustrates binding ratio as a function of FRET efficiency, inferred from the fluorescence bursts.

beam was focused into the microfluidic channel at a fixed point downstream of the dilution chamber. Emitted photons were collected using a microscope objective and focused onto an avalanche photodiode detector. The analytical concentration of each droplet was calculated from the measured fluorescence intensity. Figure 2a demonstrates the excellent correspondence between the measured droplet concentrations and the designed dilution ratio (solid line). Significantly, the concentration gradient formed can cover four orders of magnitude in a single experiment and was limited only by the achievable limit of detection. Moreover, by changing the droplet size or sample concentration in the subsequent droplets, a variety of dilution ratios or baselines were achieved readily. For example, Fig. 2b shows two droplet concentration gradients formed using an identical mother droplet with either pure solvent dilution droplets or dilution droplets at 20% of the mother droplet concentration. Such operational flexibility is especially useful in screening applications where the analytical response shows a complex dependency on concentration. This flexibility is exemplified in a study of the self-quenching behaviour of carboxyfluorescein in aqueous solutions (Supplementary Figs S6,S7).

It is recognized that the majority of chemical and biological assays require the dilution of one or more reagents when characterizing parameters such as reaction kinetics, efficiency and toxicity[5]. To this end, we used a DNA-binding homogeneous assay based on fluorescence resonance energy transfer (FRET) as a model system to demonstrate the operational utility of the dilution platform and its integration with other functional components[31]. Figure 3a illustrates the fluidic scheme. Here a FRET donor (mother) droplet contains 100 nM streptavidin labelled with Alexa Fluor 488 (AF488). Initially, this mother droplet was diluted into a sequence of 3 nl droplets of decreasing concentrations. Subsequently, these droplets were merged with a continuous stream of 20 nM single-stranded DNA (ssDNA) to generate a larger merged droplet. The ssDNA was biotinylated and labelled with the FRET acceptor AF647. Each merged droplet had a volume of 4 nl, which generated an effective DNA concentration of 5 nM with an initial streptavidin concentration of 75 nM. An incubation time of 26 seconds (between the point of merging and detection) ensured complete mixing within the droplets. The fluorescence signature (in both red and green channels) occurred as the droplet transited the optical probe volume, and the spectrally resolved emission was acquired through the use of a dichroic filter and two avalanche photodiodes, as shown in Fig. 3c.

The precise concentration of the donor was inferred directly from the green fluorescence signal (originating solely from AF488) (Fig. 3c). The concentration of the acceptor was inferred from the red fluorescence signal of AF647 with no streptavidin in the droplet. FRET signals were obtained by subtracting the contribution of AF647 to the red signal from the contribution of the diluted DNA sample. This yielded the baseline above which fluorescence reports actual FRET events. Accordingly, the correspondence of the FRET signal and the binding ratio, defined as the ratio of DNA concentration to streptavidin concentration, can be determined experimentally. This binding ratio can be used to derive binding properties based on FRET efficiency[31].

As shown in the insert of Fig. 3c, the FRET efficiency rapidly increases as a function of binding ratio with a subsequent levelling off after a threshold value of approximately one. This behaviour indicates that the number of biotin binding sites occupied by biotinylated DNA is between one and two. This result agrees with previously published results based on the same assay[31]. After the threshold binding ratio, the FRET efficiency plateaus at 50%. This is higher than the theoretical FRET efficiency of 40% defined by equation (3) with $R_0 = 39$ Å and $R_{DA} = 41.6$ Å:

$$E_{theory} = \frac{1}{(R_{DA}/R_0)^6} \quad (3)$$

Here R_0 is the characteristic Förster distance and R_{DA} is the distance between donor and acceptor. This discrepancy can be explained by the high number of fluorophores per streptavidin (approximately five). Accordingly, this type of assay can provide high-throughput molecular information on binding-site occupancy and dye–molecule interactions. Moreover, the logarithmic nature of this dilution scheme allows the collection of many data points in the regime of extreme binding ratios. This is normally difficult to achieve using conventional continuous-flow approaches. Also, although the second inlet incorporated a continuous flow, a droplet approach can be adapted easily. Accordingly, the dilution device minimizes not only the amount of compound to be screened, but also the target molecules consumed; this provides a direct route to high-throughput screening of rare samples. The output droplets can be detected directly on-chip (as shown herein) or stored within an internal or external device for applications that require a long period of incubation, such as cell culturing or crystallization.

Conclusion

In summary, we have demonstrated a new technique for the high-throughput dilution and screening of nanolitre droplets in microfluidic channels. In contrast to conventional microfluidic-based screening methods that utilize microlitre volumes of compounds and substrates, our approach requires only nanolitres at most and (in a non-optimized format) has a similar throughput to that of state-of-the-art liquid-handling technologies. The entire screening process is performed in a passive and sequential manner, and other droplet-manipulation processes (such as droplet splitting and sorting) can be integrated with ease. Also, other routine screening applications can be performed using this platform (for example, titrations, pH screening and mapping of crystallization conditions) and we will report on these in future publications. Through parallelization, screening of large compound libraries will be facilitated, and it is expected that this inexpensive chip-level screening technology has the potential to replace current expensive high-throughput screening platforms.

Methods

Chip fabrication. The microfluidic devices used for all experiments were fabricated in poly(dimethylsiloxane) (PDMS) by single-layer soft lithography[3] and bonded to a flat layer of PDMS by plasma bonding (Harrick Plasma) for one minute. The bonded chips were ready to use after being kept in a 65 °C oven overnight.

Fluidics. A precision syringe pump (PHD 2000, Harvard) was used to generate and manoeuvre droplets along the fluidic network. The pump was used in refill mode and operated at a rate of 2 μl min^{-1}. A second pump was used to inject the DNA solution at a volumetric flow rate of 0.2 μl min^{-1}. For the initial system characterization, deionized water that contained a food dye or a binding buffer was used as the aqueous phase and FC-40 with 0.75 weight% 1H,1H,2H,2H-perfluorooctanol as the oil phase. The dilution channel was rinsed with oil for ten minutes before use.

FRET assay. AF488 streptavidin conjugate was obtained from Invitrogen. The biotinylated oligonucleotide strand had the sequence biotin-5′-CGCTAAAATTATTTATTGATCGATTTTTTTTCGGGCGCGGCGGGC-3′ (Operon). The complementary strand internally modified with AF 647 was 3′-CGCG[Alexa647]TTTTAATAAATAACTAGCTAAAAAAAAGCCCGCGCC GCCCG-5′. These two strands were hybridized to produce the FRET acceptor. Hybridization was performed using a binding buffer of 100 mM Tris–HCl, 10 mM NaCl and 3 mM $MgCl_2$ at pH 8.0, and a mixture of ssDNA (biotin-labelled DNA and Alexa 647-labelled DNA) was prepared, with a final concentration of 100 nM for both strands. The DNA mixture was hybridized using a Genius Thermal Cycler (Techne, Cambridge) by quickly ramping the temperature to 92 °C and holding it for two minutes. The temperature was then slowly decreased to 4 °C at a rate of 1.6 °C min^{-1}.

For the FRET experiments described herein, the initial concentrations of labelled streptavidin and labelled biotinylated DNA were 100 nM and 20 nM, respectively. After merging, droplets that contained DNA and streptavidin were incubated for 26 seconds with the use of a long serpentine output channel.

Optics. A continuous-wave diode laser operating at 488 nm was introduced into the microfluidic channel via a dichroic mirror (505DRLP02, Omega Optical) and ×20 objective. Fluorescence photons were collected via the same objective and an emission filter (515 EFLP, Omega Optical) was used to further filter the excitation light before it was focused to a precision pinhole (75 μm, Thor Labs, Ely, Cambridgeshire). A second dichroic mirror (630DCXR) split and directed the signal onto two avalanche photodiodes (AQR-141, EG&G, Perkin-Elmer). Both detectors were linked to a DAQ device (National Instruments, USB-6251) with 50 μs resolution per channel.

Received 21 September 2010; accepted 5 April 2011; published online 23 May 2011

References

1. Hertzberg, R. P. & Pope, A. J. High-throughput screening: new technology for the 21st century. *Curr. Opin. Chem. Biol.* **4,** 445–451 (2000).
2. Sundberg, S. A. High-throughput and ultra-high-throughput screening: solution- and cell-based approaches. *Curr. Opin. Biotechnol.* **11,** 47–53 (2000).
3. Xia, Y. N. & Whitesides, G. M. Soft lithography. *Ann. Rev. Mater. Sci.* **28,** 153–184 (1998).
4. Unger, M. A., Chou, H. P., Thorsen, T., Scherer, A. & Quake, S. R. Monolithic microfabricated valves and pumps by multilayer soft lithography. *Science* **288,** 113–116 (2000).
5. deMello, A. J. Control and detection of chemical reactions in microfluidic systems. *Nature* **442,** 394–402 (2006).
6. Thorsen, T., Maerkl, S. J. & Quake, S. R. Microfluidic large-scale integration. *Science* **298,** 580–584 (2002).
7. Gomez-Sjoberg, R., Leyrat, A. A., Pirone, D. M., Chen, C. S. & Quake, S. R. Versatile, fully automated, microfluidic cell culture system. *Anal. Chem.* **79,** 8557–8563 (2007).
8. Hansen, C. L., Skordalakes, E., Berger, J. M. & Quake, S. R. A robust and scalable microfluidic metering method that allows protein crystal growth by free interface diffusion. *Proc. Natl Acad. Sci. USA* **99,** 16531–16536 (2002).
9. Jeon, N. L. *et al.* Generation of solution and surface gradients using microfluidic systems. *Langmuir* **16,** 8311–8316 (2000).
10. Dertinger, S. K. W., Chiu, D. T., Jeon, N. L. & Whitesides, G. M. Generation of gradients having complex shapes using microfluidic networks. *Anal. Chem.* **73,** 1240–1246 (2001).
11. Chung, B. G. *et al.* Human neural stem cell growth and differentiation in a gradient-generating microfluidic device. *Lab Chip* **5,** 401–406 (2005).
12. Stone, H. A., Stroock, A. D. & Ajdari, A. Engineering flows in small devices: microfluidics toward a lab-on-a-chip. *Ann. Rev. Fluid Mech.* **36,** 381–411 (2004).
13. Makamba, H., Kim, J. H., Lim, K., Park, N. & Hahn, J. H. Surface modification of poly(dimethylsiloxane) microchannels. *Electrophoresis* **24,** 3607–3619 (2003).
14. Song, H., Chen, D. L. & Ismagilov, R. F. Reactions in droplets in microfluidic channels. *Angew. Chem. Int. Ed.* **45,** 7336–7356 (2006).
15. Thorsen, T., Roberts, R. W., Arnold, F. H. & Quake, S. R. Dynamic pattern formation in a vesicle-generating microfluidic device. *Phys. Rev. Lett.* **86,** 4163–4166 (2001).
16. Anna, S. L., Bontoux, N. & Stone, H. A. Formation of dispersions using 'flow focusing' in microchannels. *Appl. Phys. Lett.* **82,** 364–366 (2003).
17. Song, H. & Ismagilov, R. F. Millisecond kinetics on a microfluidic chip using nanoliters of reagents. *J. Am. Chem. Soc.* **125,** 14613–14619 (2003).
18. Brouzes, E. *et al.* Droplet microfluidic technology for single-cell high-throughput screening. *Proc. Natl Acad. Sci. USA* **106,** 14195–14200 (2009).
19. Link, D. R. *et al.* Electric control of droplets in microfluidic devices. *Angew. Chem. Int. Ed.* **45,** 2556–2560 (2006).
20. Prakash, M. & Gershenfeld, N. Microfluidic bubble logic. *Science* **315,** 832–835 (2007).
21. Niu, X., Gulati, S., Edel, J. B. & deMello, A. J. Pillar-induced droplet merging in microfluidic circuits. *Lab Chip* **8,** 1837–1841 (2008).
22. Niu, X. Z., Gielen, F., deMello, A. J. & Edel, J. B. Electro-coalescence of digitally controlled droplets. *Anal. Chem.* **81,** 7321–7325 (2009).

23. Tan, Y. C., Fisher, J. S., Lee, A. I., Cristini, V. & Lee, A. P. Design of microfluidic channel geometries for the control of droplet volume, chemical concentration, and sorting. *Lab Chip* **4,** 292–298 (2004).
24. Niu, X. Z. *et al.* Droplet-based compartmentalization of chemically separated components in two-dimensional separations. *Chem. Commun.* 6159–6161 (2009).
25. Garstecki, P., Fuerstman, M. J., Stone, H. A. & Whitesides, G. M. Formation of droplets and bubbles in a microfluidic T-junction – scaling and mechanism of break-up. *Lab Chip* **6,** 437–446 (2006).
26. Bremond, N., Thiam, A. R. & Bibette, J. Decompressing emulsion droplets favors coalescence. *Phys. Rev. Lett.* **100,** 024501 (2008).
27. Shi, W. W., Qin, J. H., Ye, N. N. & Lin, B. C. Droplet-based microfluidic system for individual *Caenorhabditis elegans* assay. *Lab on a Chip* **8,** 1432–1435 (2008).
28. Fidalgo, L. M., Abell, C. & Huck, W. T. S. Surface-induced droplet fusion in microfluidic devices. *Lab Chip* **7,** 984–986 (2007).
29. Ottino, J. M. *The Kinematics of Mixing: Stretching, Chaos, and Transport* (Cambridge Univ. Press, 1989).
30. Tice, J. D., Song, H., Lyon, A. D. & Ismagilov, R. F. Formation of droplets and mixing in multiphase microfluidics at low values of the Reynolds and the capillary numbers. *Langmuir* **19,** 9127–9133 (2003).
31. Srisa-Art, M., deMello, A. J. & Edel, J. B. High-throughput DNA droplet assays using picoliter reactor volumes. *Anal. Chem.* **79,** 6682–6689 (2007).

Acknowledgements

This work was partially supported by the Research Councils UK Basic Technology Programme (Grant EP/D048664/1) and the National Research Foundation of Korea (Grant Number R11-2009-044-1002-0K20904000004-09A050000410).

Author contributions

X.N. conceived the dilution module, X.N., F.G., J.B.E. and A.J.D. designed the experiments, X.N. and F.G. performed the experiments, X.N., J.B.E. and F.G. analysed the data, and X.N. and A.J.D. co-wrote the manuscript. All authors discussed the results and commented on the manuscript.

Additional information

The authors declare no competing financial interests. Supplementary information accompanies this paper at www.nature.com/naturechemistry. Reprints and permission information is available online at http://www.nature.com/reprints/. Correspondence and requests for materials should be addressed to J.B.E. and A.J.d.